Lithium Ion Conductivity in New Perovskite Oxides $[Ag_yLi_{1-y}]_{3x}La_{2/3-x}\square_{1/3-2x}TiO_3$ ($x = 0.09$ and $0 \leq y \leq 1$)

O. Bohnke,* C. Bohnke, J. Ould Sid'Ahmed, M. P. Crosnier-Lopez, H. Duroy, F. Le Berre, and J. L. Fourquet

Laboratoire des Fluorures (UMR 6010 CNRS), Université du Maine, Avenue O. Messiaen, 72085 Le Mans Cedex 09, France

Received October 23, 2000. Revised Manuscript Received January 22, 2001

New perovskite-type lithium ion conductors $[Ag_yLi_{1-y}]_{3x}La_{2/3-x}TiO_3$ were synthesized and their crystal structure and ionic conductivity were characterized. The La^{3+} and vacancies contents have been fixed ($x = 0.09$) and the substitution of Ag^+ for Li^+ was varied from 0 to 1. The X-ray powder diffraction analysis revealed that the symmetry of the doubled-perovskite lattice changes from tetragonal for the nonsubstituted oxide ($y = 0$) to orthorhombic when substitution occurs ($0 < y < 1$), to come back to tetragonal when substitution is complete ($y = 1$). The substitution leads to changes in the bottleneck sizes and form of the two different A-cages of the structure and consequently to the lowest activation energy of the conduction process ever found in these titanates ($E_a = 0.28$ eV for $y = 0.5$). The immobile ions (La^{3+} and Ag^+) can be considered as obstacles for the lithium motion through the conduction pathways. Conductivity measurements show that lithium and vacancies no longer percolate when the number of immobile ions per Ti in these oxides is greater than 75%. These immobile ions are distributed differently in the two perovskite subcells of the unit cell, leading to an immobile-ions(La^{3+}/Ag^+)-poor layer and an immobile-ions-rich layer. The ionic conductivity is found to follow the occupancy of the poor layer; that is, the higher the occupancy, the smaller the lithium conductivity. The lithium motion occurs then mainly in the (La^{3+}/Ag^+)-poor layer of these oxides.

Introduction

The high lithium conductivity of the perovskite-type Li-ion conductors belonging to the solid solution $Li_{3x}La_{2/3-x}TiO_3$ (LLTO) has been first reported by Belous and co-workers in 1987.[1] Much attention has been paid to these materials since the paper of Inaguma et al. in 1993, who reported an ionic conductivity of 10^{-3} S cm^{-1} for $x = 0.11$ at room temperature.[2] These authors have also shown that the lithium-ion conductivity is strongly influenced by both the site percolation and the ratio of lithium to vacancy concentration.[3] Another important factor is the conduction channel size. To migrate from one A site to the next available one, the lithium ions have to pass through a bottleneck made of four oxygens. The size of this bottleneck is the predominant factor of the activation energy for the ionic conduction.[4,5] To prepare more conductive perovskites, one possibility is then to increase the number of mobile ions and/or vacancies but another one is to decrease the activation energy. As predicted by Inaguma et al., the bottleneck size mostly influences the activation energy of the ionic motion mechanism by varying the repulsion potential between oxygen and lithium at the bottleneck site.[6]

In the perovskites (ABO_3) the skeletal of the structure is made of BO_6 octahedra where B is generally a transition metal. The arrangement of these octahedra leads to the formation of cages where A ions can be introduced. These A ions can be regarded as spacers in the structure that influence the perovskite parameter a_p and then the bottleneck size. The highest lithium conductivity at room temperature, reported until now, has been obtained with a member of the titanate solid solution (LLTO). To increase the ionic conductivity, many attempts have been described in the literature to modify the parameter a_p and then the bottleneck size. This has been performed by substitution of ions in either the A site[4,6−12] or the B site of the perovskite structure by preparing niobates,[13−17] titanates,[18−20] or mixed transition metal oxides.[4,21−24]

* To whom correspondence should be addressed. Tel.: +33-2-4383-3354. Fax: +33-2-4383-3506. E-mail: odile.bohnke@univ-lemans.fr.

(1) Belous, A. G.; Novitskaya, G. N.; Polyanetskaya, S. V.; Gornikov, Y. I. *Zh. Neorg. Khim.* **1987**, *32*, 283−286.

(2) Inaguma, Y.; Chen, L.; Itoh, M.; Nakamura, T.; Uchida, T.; Ikuta, H.; Wakihara, M. *Solid State Commun.* **1993**, *86* (10), 689−693.

(3) Inaguma, Y.; Itoh, M. *Solid State Ionics* **1996**, *86−88*, 257−260.

(4) Katsumata, T.; Matsui, Y.; Inaguma, Y.; Itoh, M. *Solid State Ionics* **1996**, *86−88*, 165−169.

(5) Inaguma, Y.; Katsumata, T.; Yu, J.; Itoh, M. *Mater. Res. Soc. Symp. Proc.* **1997**, *453*, 623−627.

(6) Inaguma, Y.; Matsui, Y.; Yu, J.; Shan, Y. J.; Nakamura, T.; Itoh, M. *J. Phys. Chem. Solids* **1997**, *58* (6), 843−852.

(7) Itoh, M.; Inaguma, Y.; Jung, W. H.; Chen, L.; Nakamura, T. *Solid State Ionics* **1994**, *70/71*, 203−207.

(8) Kawai, H.; Kuwano, J. *Ceramics: Charting the Future*, Proceedings of the 8th Cimtec World Ceramic Congress, Florence, Italy; Vincenzini, P., Ed.; 1994; pp 2641−2648.

(9) Robertson, A. D. G.; Arcia Martin, S.; Coats, A.; West, A. R. *J. Mater. Chem.* **1995**, *5* (9), 1405−1412.

(10) Morales, M.; West, A. R. *Solid State Ionics* **1996**, *91*, 33−43.

(11) Lee, J. S.; Yoo, K. S.; Kim, T. S.; Jung, H. J. *Solid State Ionics* **1997**, *98* 15−26.

(12) Harada, Y.; Watanabe, H.; Kuwano, J.; Saito, Y. *J. Power Sources* **1999**, *81−82*, 777−781.

10.1021/cm001207u CCC: $20.00
Published on Web 04/27/2001

In the noncubic oxides LLTO, the structural study performed by Fourquet et al.[25] has clearly shown that the unit cell is made by stacking two perovskite subcells. These subcells have different La^{3+} populations and different A-site sizes with different bottleneck sizes. The La^{3+}-rich layer has a smaller A-cage size than the La^{3+}-poor layer. For the analysis of the conductivity data, it is then reasonable to consider the size of the six bottlenecks present in the two subcells of the perovskite structure (i.e., two bottlenecks in each crystallographic direction, *a*, *b*, and *c*) rather than the a_p parameter that is a mean value of these subcells sizes.

The aim of this paper is then to investigate the influence of the framework of noncubic titanates obtained by substitution of Ag^+ ions for Li^+ on the lithium conductivity (i.e., presence of different subcells and distortion of the bottlenecks). The prepared oxides have the general formulation $[Ag_yLi_{1-y}]_{3x}La_{2/3-x}TiO_3$. We will focus our attention on the structural features induced by the Ag^+/Li^+ substitution and on its influence on the lithium conductivity. We have to mention that Katsumata et al. have reported substitution of Ag^+ for Li^+ in the niobate $La_xAg_yLi_{1-3x-y}NbO_3$.[16] A maximum conductivity of 3.9×10^{-5} S cm^{-1} at 300 K has been reported. The authors concluded that the nonoptimization of the lattice parameters for niobates was the reason for such a low conductivity that is mainly dominated by the activation energy.

Experimental Section

Samples Preparation. $[Ag_yLi_{1-y}]_{3x}La_{2/3-x}TiO_3$ was prepared from stoichiometric amounts of Li_2CO_3 (Aldrich, 99.99%), Ag_2CO_3 (Merck, 99.9%), TiO_2 (Riedel de Haen, 99.5%), and La_2O_3 (Rhône Poulenc, 99.999%) by solid-state reaction. La_2O_3 was dried at 1000 °C for 12 h before weighing. The reagents were mixed in a mortar. The mixture of the raw materials was pressed into pellets. They were heated at 850 °C for 4 h in a platinum crucible (to drive off CO_2) and then fired at 1050 °C for 12 h in air. The heating rate was 5 °C min^{-1}. The samples were then allowed to naturally cool in the furnace down to 200 °C. After regrinding and repressing, the samples were heated at 1100 °C for 10 h in air at a sweep rate of 5 °C min^{-1} and cooled to 200 °C followed by further grinding, repelleting, and refiring at 1150 °C for 10 h at the same sweep rate as above to complete the reaction and finally allowing to cool to 200 °C. The final pellets were 5 mm in diameter and 1−2 mm in thickness. The compactness of the pellet was around 70−75%. The metal composition of the samples (Ti, La, and Ag (in atom %)) has been analyzed by scanning electron microscopy. All the substituted samples contain Ti, La, and Ag as introduced during the preparation. For example, the atom % of La, Ti, and Ag determined by SEM at low magnification (×40), for $y = {}^2/_3$, are 34, 56, and 10% (at 1%), respectively. This corresponds to the theoretical values, which are 32.8, 56.9, and 10.2%. No Ag evaporates then at high temperature. However, for the low Ag content sample ($y = {}^1/_3$) analysis at high magnification (×10 000) reveals that Ag^+ is not homogeneously distributed in the sample.

Structural Characterization. The crystal structures of the samples were studied by X-ray powder diffraction on a D500 Siemens diffractometer at room temperature with the following experimental conditions: radiation Cu Kα, 2θ range of 5°−120°, step $\Delta 2\theta = 0.04°$, and time by step 18 s. The patterns were analyzed through the Rietveld method by using the Fullprof software.[26]

Conductivity Measurements. Conductivity measurements were carried out by the complex impedance method with a frequency response analyzer 1276 (Solartron) from room temperature to 900 K in the frequency range from 10 MHz to 1 Hz with 40 measurements per decade and an applied voltage of 100−400 mV (rms), depending on the temperature (the response of the electrochemical system remains linear up to almost 400 mV). Platinum paste was painted on both sides of the pellet as ionically blocking electrodes. The sample was mounted in a two-platinum-electrode cell and measurements were performed under dried N_2 to avoid any water contribution to the total conductivity. It was allowed to equilibrate for 1−2 h before measurement until reproducible impedance spectra were obtained. The Zview equivalent circuit software of Solartron has been used to fit the impedance spectra and determine the bulk resistance of the samples. The form factor was determined for each sample and was of the order of 0.7 cm^{-1}.

Results and Discussion

We have first prepared the compounds $Ag_{3x}La_{2/3-x}TiO_3$ by total substitution of Ag^+ ions for Li^+ ions and we have investigated their crystal structure. The X-ray diffraction patterns revealed the formation of a monophasic perovskite phase in the composition range $0.07 \leq x \leq 0.17$. These oxides did not show any ionic conductivity. Therefore, the Ag^+ ions are not able to pass through the bottlenecks available for conduction. This is due to the size of this ion (e.g., $r_{Ag^+} = 1.28$ Å in 8-coordination compared to $r_{La^{3+}} = 1.16$ Å and $r_{Li^+} = 0.92$ Å in the same coordination state[27]).

We then prepared some titanates by partial substitution of Ag^+ ions for Li^+ ions and we studied their crystal structure and ionic conductivity. We prepared five samples of general formulation $[Ag_yLi_{1-y}]_{3x}La_{2/3-x}TiO_3$ in which *x* was kept constant (i.e., $x = 0.09$) and *y*, the substitution parameter, was varied from 0 to 1. In such compounds the number of La^{3+} and vacancies remain constant. Moreover, because Li^+ and Ag^+ ions have the same valence, the mean value of the valence of the A site remains constant throughout the substitution. The *y* values were fixed to 0, ${}^1/_3$, ${}^1/_2$, ${}^2/_3$, and 1. The first compound is one member of the LLTO solid solution we have already studied,[28−31] and the last one is the totally and nonconductive substituted oxide.

(13) Kawakami, Y.; Fukuda, M.; Ikuta, H.; Wakihara, M. *Solid State Ionics* **1998**, *110*, 187−192.
(14) Kawakami, Y.; Ikuta, H.; Wakihara, M. *J. Solid State Electrochem.* **1998**, *2*, 206−210.
(15) Shan, Y. J.; Sinozaki, N.; Nakamura, T. *Solid State Ionics* **1998**, *108* 403−406.
(16) Katsumata, T.; Inaguma, Y.; Itoh, M. *Solid State Ionics* **1998**, *113−115*, 465−469.
(17) Garcia Martin, S.; Rojo, J. M.; Tsukamoto, H.; Moran, E.; Alario−Franco, M. A. *Solid State Ionics* **1999**, *116*, 11−18.
(18) Mizumoto, K.; Hayashi, S. *J. Ceram. Soc. Jpn.* **1997**, *105* (8), 713−715.
(19) Mizamoto, K.; Hayashi, S. *Solid State Ionics* **1999**, *116*, 263−269.
(20) Mizamoto, K.; Hayashi, S. *Solid State Ionics* **2000**, *117*, 241−251.
(21) Latie, L.; Villeneuve, G.; Conte, D.; Le Flem, G. *J. Solid State Chem.* **1984**, *51*, 293−299.
(22) Inaguma, Y.; Matsui, Y.; Shan, Y. J.; Itoh, M.; Nakamura, T. *Solid State Ionics* **1995**, *79*, 91−97.
(23) Watanabe, H.; Kuwano, J. *J. Power Sources* **1997**, *68*, 421−426.
(24) Chung, H. T.; Kim, J. G.; Kim, H. G. *Solid State Ionics* **1998**, *107* 153−160.
(25) Fourquet, J. L.; Duroy, H.; Crosnier-Lopez, M. P. *J. Solid State Chem.* **1996**, *127*, 283−294.
(26) Rodriguez-Carvajal, J. *FULLPROF software: Rietveld Pattern Matching Analysis of Powder Patterns*; ILL: Grenoble, 1990.
(27) Shannon, R. D. *Acta Crystallogr. Sect A* **1976**, *32*, 751.
(28) Bohnke, O.; Bohnke, C.; Fourquet, J. L. *Solid State Ionics* **1996**, *91*, 21−31.

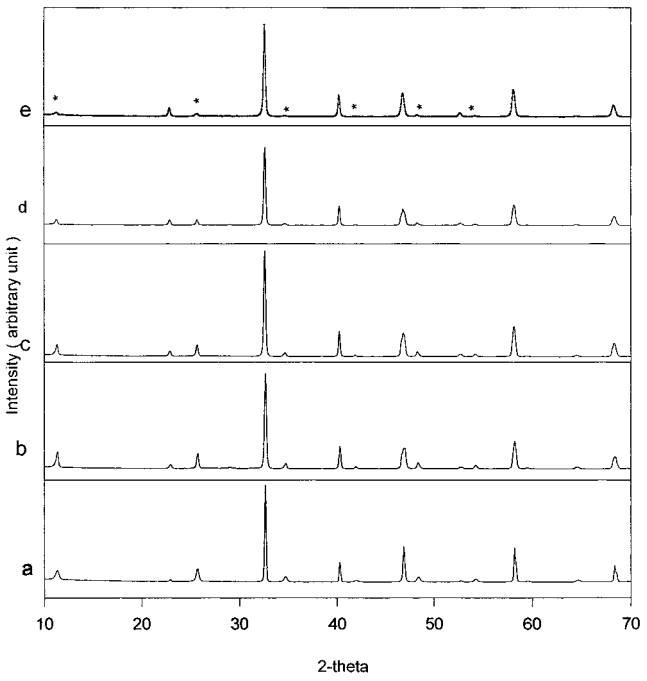

Figure 1. Powder X-ray diffraction patterns of $[Ag_yLi_{1-y}]_{3x}La_{2/3-x}TiO_3$ at room temperature for (a) $y = 0$, (b) $y = {}^1/_3$, (c) $y = 0.5$, (d) $y = {}^2/_3$, and (e) $y = 1$. The superstructure lines are marked by asterisks.

1. Crystal Structure. Figure 1a−e shows the room-temperature powder X-ray diffraction patterns of these five compounds as a function of substitution. Only patterns b and d show the presence of some impurities around $2\theta \approx 28°$. The Fullprof analysis of the patterns shows that the crystal structure changes from tetragonal for the nonsubstituted material (i.e., $y = 0$ or LLTO) to orthorhombic for $0 < y < 1$ to come back to tetragonal for $y = 1$, when substitution is complete. This symmetry modification is observed, as an example, in Figure 2 that shows the X-ray diffraction patterns, near $2\theta = 78°$, for $y = 0.5$ and $y = 1$. The splitting of the (302, 032) diffraction lines observed for $y = 0.5$ (orthorhombic symmetry) disappears for $y = 1$ (tetragonal symmetry). The refinements of the doubled-perovskite structure were obtained by using two similar structural models in the space group $P4/mmm$ for the tetragonal symmetry ($a = b \approx 3.87$ Å and $c \approx 2a$), as previously described by Fourquet et al. for LLTO[26] and $Pmmm$ for the orthorhombic one ($a \neq b$ and $c \approx 2a$) as shown in Table 1. These models are characterized by a distribution of vacancies, Li^+, La^{3+}, and Ag^+ ions over two sites (1a and 1b in $P4/mmm$, 1a and 1c in $Pmmm$). These two sites will be called La1 and La2, respectively. Because Li^+ has a small X-ray scattering factor, its contribution has been omitted in the refinement procedure. Therefore, only La^{3+} and Ag^+ ions were allowed to distribute in the two sites during refinement. Figure 3 shows for example the good agreement obtained between the observed and calculated patterns for $y = 0.5$. Figure 4 presents the variation of the lattice parameters a, b, and $c/2$ as a function of the substitution parameter y and Table 2 summarizes the results (space group, parameters, and cell volume) obtained from the structural refinement. It can be observed that the Ag^+/Li^+ substitution introduces a distortion in the unit cell.

As for LLTO, superstructure lines (with $l = 2n + 1$) are observed for all the compounds. They are indicated

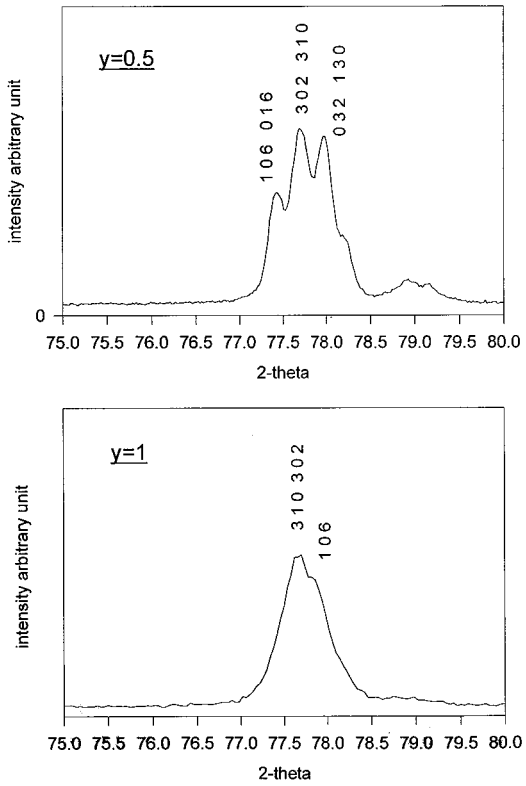

Figure 2. Variation of the line profiles near $2\theta = 78°$ for two members of the $[Ag_yLi_{1-y}]_{3x}La_{2/3-x}TiO_3$ ($x = 0.09$) solid solution: $y = 0.5$ (top) and $y = 1$ (bottom).

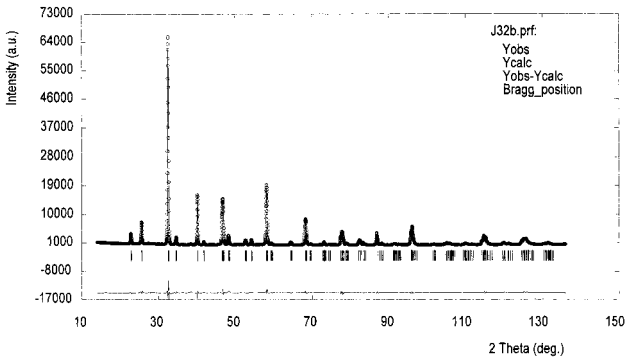

Figure 3. Calculated and (...) observed X-ray diffraction patterns for $[Ag_yLi_{1-y}]_{3x}La_{2/3-x}TiO_3$ $y = 0.5$. The difference spectrum is shown below at the same scale. Final agreement factors obtained with 327 intensities and 19 fitted parameters: $R_p = 5.91\%$, $R_{wp} = 8.07\%$, $\chi^2 = 6.97$.

Table 1. $[Ag_yLi_{1-y}]_{3x}La_{2/3-x}TiO_3$ ($x = 0.09$): Structural Model in the Space Group $Pmmm$ (No. 47)

atom	position	atomic coordinates (x, y, z)
La1 (La^{3+}, Ag^+, Li^+, □)	1a	(0, 0, 0)
La2 (La^{3+}, Ag^+, Li^+, □)	1c	(0, 0, ${}^1/_2$)
Ti	2t	(${}^1/_2$, ${}^1/_2$, z) $z \approx 0.25$
O1	2s	(${}^1/_2$, 0, z) $z \approx 0.25$
O2	2r	(0, ${}^1/_2$, z) $z \approx 0.25$
O3	1f	(${}^1/_2$, ${}^1/_2$, 0)
O4	1h	(${}^1/_2$, ${}^1/_2$, ${}^1/_2$)

(29) Emery, J.; Buzare, J. Y.; Bohnke, O.; Fourquet, J. L. *Solid State Ionics* **1997**, *99*, 41−51.
(30) Bohnke, O.; Emery, J.; Veron, A.; Fourquet, J. L.; Buzare, J. Y.; Florian, P.; Massiot, D. *Solid State Ionics* **1998**, *109*, 25−34.
(31) Emery, J.; Bohnke, O.; Fourquet, J. L.; Buzare, J. Y.; Florian, P.; Massiot, D. *J. Phys.: Condens. Matter* **1999**, *11*, 10401−10417.

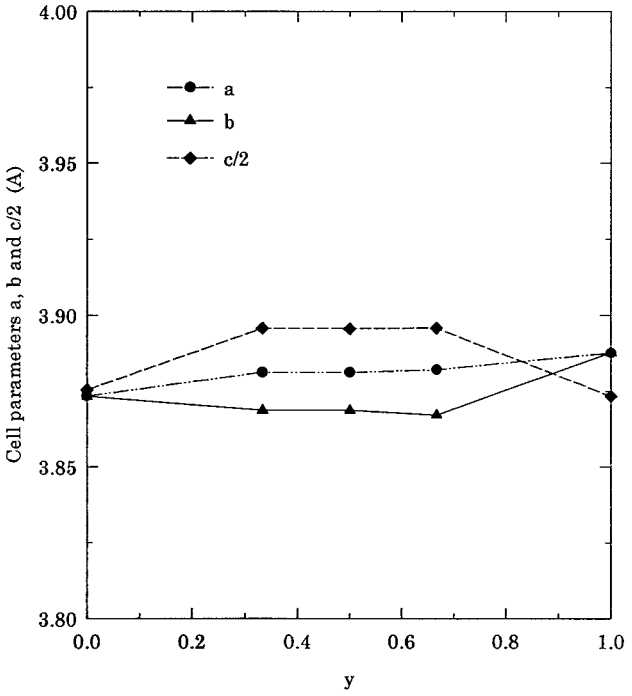

Figure 4. Evolution of the lattice parameters *a*, *b*, and *c*/2 as a function of the substitution parameter *y*.

Table 2. Space Group, Parameters, and Volume of the Unit Cell in Cubic Angstroms for $[Ag_yLi_{1-y}]_{3x}La_{2/3-x}TiO_3$ ($x = 0.09$) as a Function of *y*

y	space group	*a* (Å)	*b* (Å)	*c* (Å)	*V* (Å^3) ± 0.02
0 (LLTO)	*P*4/*mmm*	3.873(3)	3.873(3)	7.750(8)	116.28
1/3	*Pmmm*	3.881(2)	3.868(7)	7.791(4)	116.99
1/2	*Pmmm*	3.881(2)	3.868(7)	7.791(1)	116.99
2/3	*Pmmm*	3.882(0)	3.867(1)	7.791(6)	116.97
1	*P*4/*mmm*	3.887(6)	3.887(6)	7.746(5)	117.08

in Figure 1e as (*). They indicate a doubling of the *c*-axis parameter. It can be observed in Figure 1 that the intensity of these superstructure lines varies with substitution. They become less intense but do not broaden as *y* increases. According to the paper of Fourquet et al. on LLTO (space group *P*4/*mmm*),[25] the existence of these superstructure lines is explained by an unequal distribution of La^{3+} ions over the (0,0,0) and (0,0,1/2) A sites of the unit cell leading to the existence of a La^{3+}-rich layer (La1) and a La^{3+}-poor layer (La2), respectively. In the substituted compounds and according to the structural models described previously, the structural refinement leads to the determination of the population of La^{3+} and Ag^+ in the two (0,0,0) and (0,0,1/2) A sites of the unit cell. Figures 5a and 5b show the evolution of the populations of La^{3+}, Ag^+, and (Li^+ and vacancies) as a function of *y*. Because Ag^+ is not mobile in these oxides, both La^{3+} and Ag^+ are immobile ions and then can be viewed as spacers in the oxide structure. Figure 5 shows that, in these compounds, as in LLTO, there is an immobile-ions-rich layer, the (0,0,0) A-site layer (or La1), and an immobile-ions-poor layer, the (0,0,1/2) A-site layer (or La2). The introduction of Ag^+ instead of Li^+ changes the repartition of the La^{3+} ions between the two layers. The La^{3+} content in the (0,0,0) A site decreases as *y* increases. On the other hand, the La^{3+} content in the (0,0,1/2) A site increases as *y* increases. This can be due to the bigger size of the Ag^+ ion compared to the Li^+ one because both of them have the same valence.

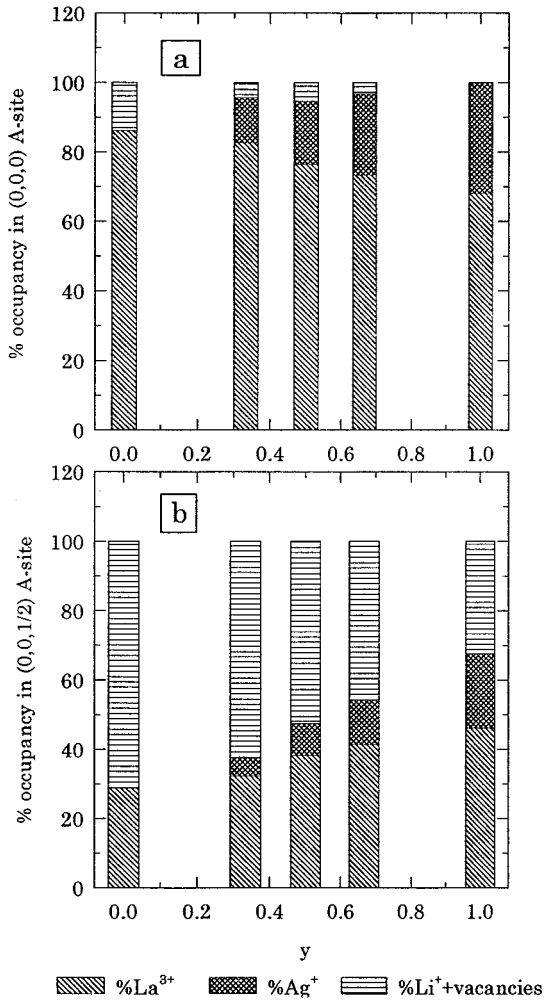

Figure 5. Evolution of the La^{3+}, Ag^+, and (Li^+ and vacancies) in the two A sites of the structure as a function of substitution parameter *y*: (a) in the (0,0,0)-rich layer and (b) in the (0,0,1/2)-poor layer.

Moreover, the number of immobile ions (i.e. La^{3+} and Ag^+) increases in both layers. The ratio of the number of immobile ions in La1 to the number of immobile ions in La2 decreases as *y* increases; the population tends to equalize. The tendency of the immobile ions population to equalize leads to a decrease of the superstructure lines area. This is in good agreement with the experimental results of Fourquet et al.[25] who found that the superstructure lines area decreases as the lithium content increases. The increase of Li^+ content in both oxides, that is, LLTO or Ag^+/Li^+ oxides, is accompanied by the same evolution of the La^{3+} population in the two A sites.[25] This confirms the assumption that the intensity of these superstructure lines are directly linked to the La^{3+}/Ag^+ ions and to their distribution between the two layers. The higher the difference between the population of the two layers, the more intense are the superstructure lines. Much care has to be taken when the intensity of the superstructure lines is considered. Indeed, the intensity is linked not only to the La^{3+}/Ag^+ population in the two layers but also to the disorder in the stacking of the La1 and La2 layers. The higher this disorder, the broader and less intense the superstructure lines. Consequently, different populations of im-

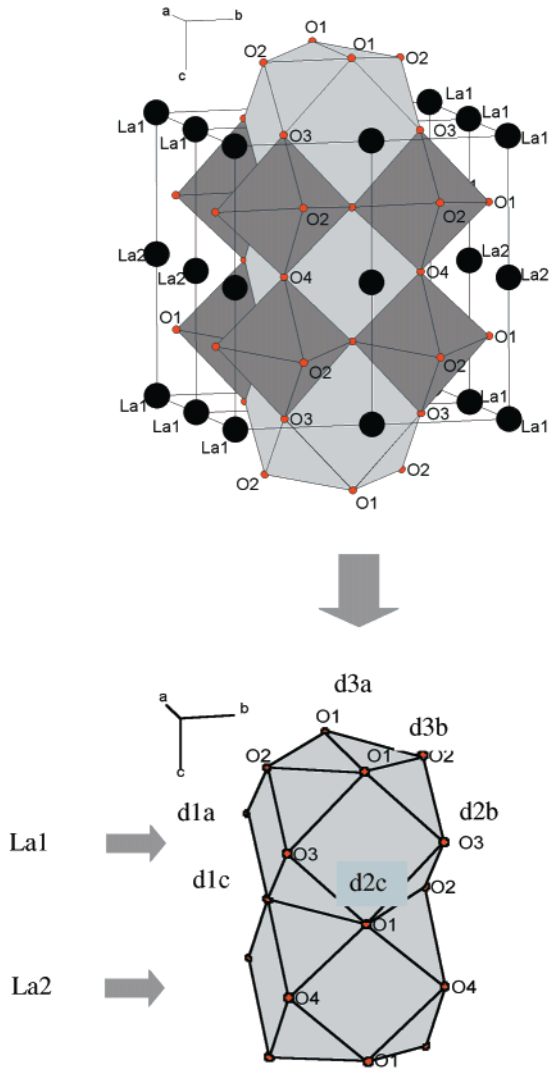

Figure 6. Stacking of the two A cages of the doubled-perovskite unit cell.

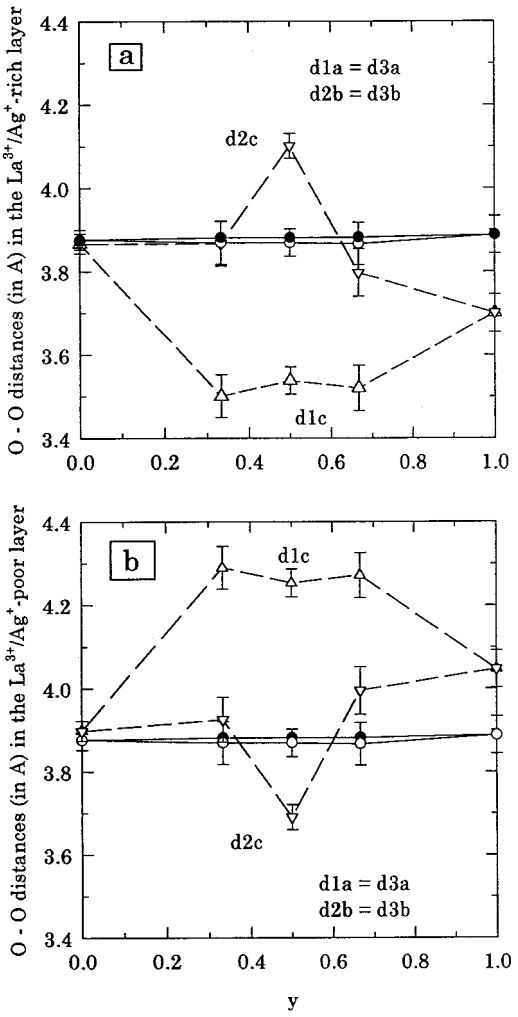

Figure 7. Evolution of the six oxygen−oxygen distances of the bottlenecks in the two A sites of the structure as a function of substitution parameter *y*: (a) in the (0,0,0)-rich layer and (b) in the (0,0,1/2)-poor layer. d1*a* and d1*c* refer to the face parallel to the (*a*,*c*) direction, d2*b* and d2*c* to the face parallel to the (*b*,*c*) direction, and d3*a* and d3*b* to the face parallel to the (*a*,*b*) direction. (the absolute error = 3 × estimated standard deviation (esd)).

mobile ions in the two layers associated with an important disorder of the stacking of these layers leads to very broad superstructure lines.

Table 2 shows that the volume of the unit cell varies very slightly when *y* increases. This is due to the sizes of La^{3+} and Ag^{+} ions, which are not very different. La^{3+} and Ag^{+} act as spacers of the unit cell and the substitution of Ag^{+} for Li^{+} increases very slightly the volume of the unit cell. However, it can be observed that if the volume of the unit cell remains almost constant, the size and the form of the two A cages vary with the Ag^{+} content. Figure 6 shows the stacking of the two different A cages forming the unit cell. In each cage there are six bottlenecks available for the Li^{+} ions to pass through. According to Figure 6, Li^{+} ions can move in the *b* direction through the faces (1) parallel to the (0,1,0) plane, in the *a* direction through the faces (2) parallel to the (1,0,0) plane or in the *c* direction through the faces (3) parallel to the (0,0,1) plane. All the bottlenecks are made of four oxygens and the distances between two oxygens are referred to as d1*a* and d1*c* for the faces (1) in the (0,1,0) plane, d2*b* and d2*c* for the faces (2) in the (1,0,0) plane, and d3*a* and d3*b* for the faces (3) in the (0,0,1) plane. For the oxides with the tetragonal structure (i.e., $y = 0$ and $y = 1$) faces (1) and (2) are identical and the four oxygens forming a bottleneck are in the same plane. In the *a* and *b* directions the oxygen atoms form lozenges and in the *c* direction they form a square. For the oxides with the orthorhombic structure ($y \neq 0$ and $y \neq 1$), the pathways of the Li^{+} ions are different in the three directions. In the *a* and *b* directions the ions have to pass through faces made of four oxygens in the same plane forming lozenges. In the *c* direction the Li^{+} ions have to pass through distorted planes (3) made of four oxygens (i.e., d1*c* ≠ d2*c*). Figure 7a,b shows the oxygen−oxygen distances for the two A cages (0,0,0) and (0,0,1/2), respectively. The error bars shown in this figure take into account the fact that the position of the O1 and O2 oxygen atoms are obtained from the Rietveld analysis of the X-ray diffraction patterns with some uncertainty. It can be noticed that better results would be obtained by neutron diffraction. However, it can be seen in Figure 7 that the variations of the d1*c* and d2*c* distances are not due to the errors in the determination of the O positions in the refinement of the structure. The Ag^{+} substitution does not change the size of the bottlenecks in the *a* and *b* directions.

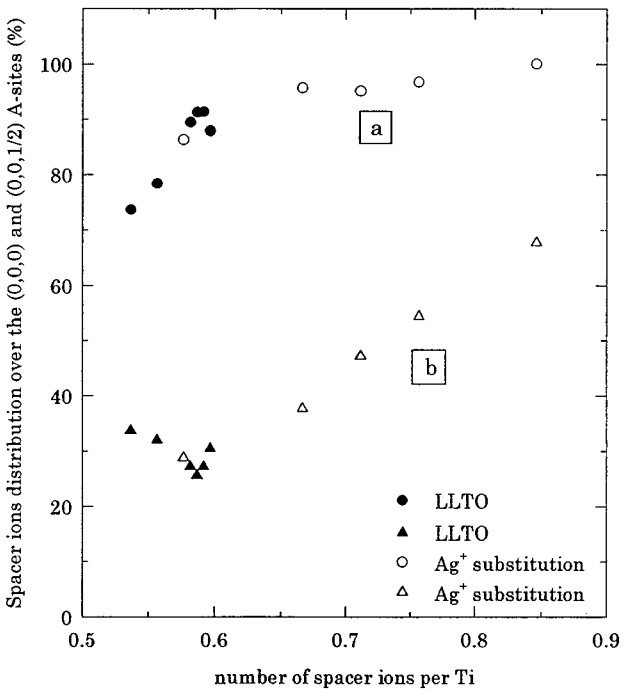

Figure 8. Evolution of the immobile or spacer ions (La^{3+} and Ag^{+}) distribution, in % occupancy of the site, in the two A sites of the structure as a function of number of spacer ions per Ti: (a) in the (0,0,0)-rich layer and (b) in the (0,0,$^1/_2$)-poor layer.

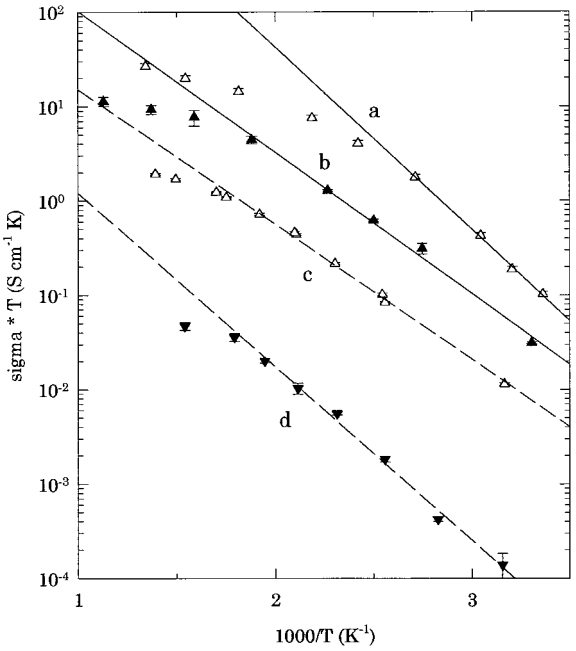

Figure 9. Logarithmic plot of the dc conductivity as a function of the inverse of temperature for $[Ag_yLi_{1-y}]_{3x}La_{2/3-x}TiO_3$ for (a) $y = 0$, (b) $y = {}^1/_3$, (c) $y = 0.5$, and (d) $y = {}^2/_3$. (Symbols = experimental data; lines = linear regression fitting).

However, in the *c* direction, d1*c* and d2*c* vary greatly with substitution in the opposite direction in each cage, leading to an almost constant volume, as shown in Table 2. The A cages of the immobile-ions-poor layer are bigger than the A cages of the immobile-ions-rich layer, suggesting that the lithium motion is more probable in the (0,0,0) layer than in the (0,0,$^1/_2$) one.

The substitution of Ag^+ for Li^+ changes the form and the size of the A cages and then the bottlenecks through which the Li^+ ions have to move. It also changes the La^{3+} population of the layers La1 and La2. Because Ag^+ and La^{3+} have almost the same ionic radius and because they are not mobile in the structure, we can conclude that the substitution increases the number of spacers in the structure and decreases the number of mobile Li^+ ions, as did the substitution of La^{3+} for $3Li^+$ in LLTO. Figure 8 shows the evolution of the immobile ions distribution (i.e., La^{3+} and Ag^+) in % occupancy over the two A sites (0,0,0) and (0,0,$^1/_2$) as a function of the number of spacer ions per Ti for both LLTO, according to previous studies,[25] and for the herein studied oxides. The two curves show continuous behavior, suggesting that the distribution of the spacers over the two layers are directly linked to the size of these spacers. The valence of the spacers may affect the form of the A cages as shown by the change of structure. For the rich layer the population increases to reach a 100% value. However, for the poor layer, the population first decreases and then increases. The small number of vacancies present in the rich layer suggests that Li^+ ions do not move inside this layer. These ions can then move inside the immobile-ions-poor layer in the *a* and *b* directions and from one layer to the other in the *c* direction. The probability for a lithium ion to move in the *c* direction may become smaller and smaller as substitution occurs because the occupancy of the rich layer tends to reach 100%.

2. dc Conductivity. Figure 9 shows the dc conductivity data expressed as $\log(\sigma^*T)$ as a function of the inverse of the temperature for $^1/_3 \le y \le 1$. The experimental errors (of the order of 7%) are shown as error bars in the plot (they are of the same size as the symbols). As previously shown for LLTO,[28] these data do not follow an Arrhenius law at high temperatures. This feature has not been clearly explained but may be related to the correlation effects between mobile ions. From the linear part of these plots the activation energy, E_a, and the pre-exponential factor, σ_0, are determined by a linear regression to a first order (lines in the plots). Table 3 summarizes these results with the correlation coefficient r^2 obtained for these regressions and the temperature range used for the fitting. The errors for E_a and σ_0 are also reported in Table 3.

Table 3 shows that the substitution of Ag^+ for Li^+ leads to a decrease of the dc conductivity to lead to a

Table 3. dc Conductivity at 300 K, Preexponential Factor σ_0, and Activation Energy E_a for $[Ag_yLi_{1-y}]_{3x}La_{2/3-x}TiO_3$ ($x = 0.09$) As a Function of y

y	σ (S cm^{-1}) at 300 K (6%)	σ_0 (S cm^{-1} K) (20%)	E_a (eV)	correlation coefficient r^2	temp range (°C) for the linear regression
0 (LLTO)	3.4×10^{-4}	3.1×10^5	0.38 ± 0.02	0.9984	100−25
$^1/_3$	10^{-4}	5.0×10^3	0.30 ± 0.02	0.9934	260−30
0.5	2.3×10^{-5}	3.5×10^2	0.284 ± 0.007	0.9956	300−40
$^2/_3$	2×10^{-7}	68	0.365 ± 0.007	0.9942	280−40
1	no conductivity				

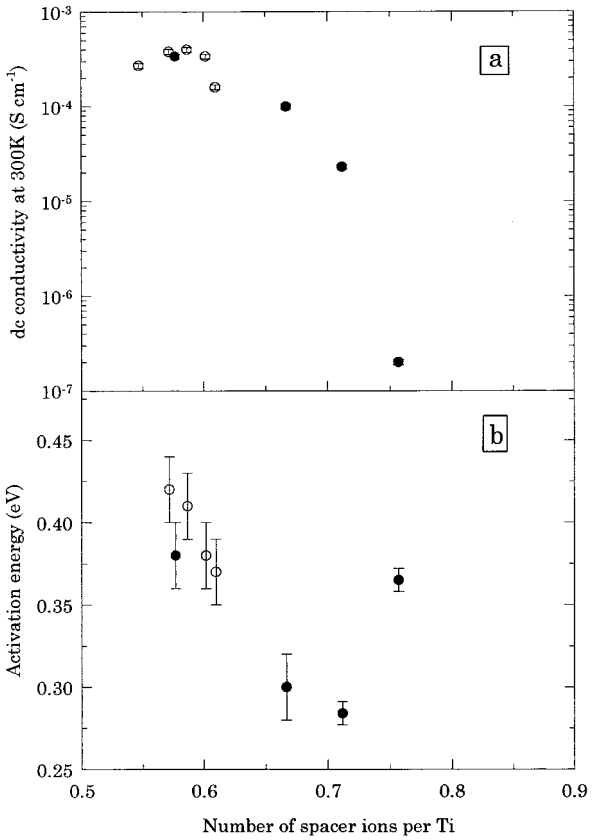

Figure 10. (a) Room-temperature dc conductivity; (b) activation energy (eV) as a function of the number of spacer ions (La^{3+} and Ag^{+}) per Ti for (○) $Li_{3x}La_{2/3-x}TiO_3$ and (●) $[Ag_yLi_{1-y}]_{3x}La_{2/3-x}TiO_3$.

nonconductive oxide when substitution is greater than $^2/_3$. This decrease of conductivity is mainly due to a decrease of the number of mobile ions as shown by the values of the pre-exponential factor. Indeed, the activation energy decreases at the beginning of the substitution (for $y \leq 0.5$). Therefore, a better conductivity could be achieved by increasing slightly the x value in these studied oxides to keep low activation energy and to increase the number of mobile ions.

Figure 10a shows the dc conductivity at room temperature as a function of the number of immobile ions (or spacers ions) per Ti for both LLTO[28] and the herein studied substituted oxides. A maximum of the dc conductivity is observed in LLTO for $x = 0.11$. Afterward, conductivity decreases with substitution when the number of immobile ions increases. The form of this curve can be compared to the curve b of Figure 8 for the spacer ions distribution in the poor layer. The similarity of the form of these two curves suggests that the occupancy of the immobile-ions-poor layer is the predominant factor for the ionic conductivity and that this conductivity occurs mainly in the *a* and *b* directions. The sudden decrease of conductivity for 75% of immobile ions per Ti in the structure is due to the site percolation phenomenon. Figure 10a shows that if the carrier concentration (lithium + vacancies) is smaller than 25% in this distorted structure, the lithium ions and vacancies no longer percolate through the system. A threshold carrier concentration of 0.3117 is reported for a simple cubic lattice[32] and 0.30 by Inaguma et al. for LLTO.[3] Our result is in good agreement with these values.

Figure 10b presents the activation energy E_a as a function of the number of immobile ions (or spacers ions) per Ti for LLTO from ref 28 and for the herein studied substituted oxides. For all the conductive substituted compounds the activation energy is smaller than the LLTO one and for $y = 0.5$ it is the smallest ever reported in the literature for either titanates, niobates, or tantalates.[16] This suggests that, as shown in Figure 7a, the activation energy is directly linked to the size of the bottlenecks. A maximum distortion of the face (3) is found for $y = 0.5$, that is, d1*c* is maximum and d2*c* is minimum in the immobile-ions-poor layer and d1*c* is minimum and d2*c* is maximum in the immobile-ions-rich layer. The face (1) of this poor layer is then big enough for the lithium to pass through. Indeed, it is greater than the oxygen and lithium ionic diameters (i.e., 3.98 Å). The radius of the O^{2-} ion in 2-coordination number is 1.40 Å and the radius of Li^{+} in 4-coordination number is 0.59 Å.[27] Such an important distortion leads to minimization of the activation energy of the mechanism of conduction by decreasing the repulsive interaction between the Li^{+} ion and the four O^{2-} ions at the bottleneck site.

Conclusions

In this study the influence of the size of the bottlenecks and form on the lithium conductivity in perovskite-type titanates has been shown. The substitution of Ag^{+} for Li^{+} changes the location of the oxygen ions of the framework and leads to a distortion of the bottlenecks. Such a distortion is favorable for the conduction mechanism because it decreases the activation energy. It has also been shown that the lithium motion occurs mainly in the immobile-ions-poor layer of the doubled-perovskite unit cell because the conductivity follows the occupancy of this layer. The higher the occupancy, the smaller the ionic conductivity. The modulation of the population of these layers seems to be an important parameter for the lithium conductivity in these oxides.

CM001207U

(32) Aharony, A. *Introduction to Percolation Theory*, 2nd ed.; Taylor and Francis: London, 1992.